Check for updates

OPEN

Fluorescent aminal linked porous organic polymer for reversible iodine capture and sensing

Muhammad A. Sabri[1], Mohammad H. Al-Sayah[2], Susan Sen[2], Taleb H. Ibrahim[1] & Oussama M. El-Kadri[2]✉

A novel triazene-anthracene-based fluorescent aminal linked porous organic polymer (TALPOP) was prepared via metal free-Schiff base polycondensation reaction of 9,10-bis-(4,6-diamino-S-triazin-2-yl)anthracene and 2-furaldehyde. The polymer has exceptional chemical and thermal stabilities and exhibit good porosity with Brunauer–Emmett–Teller surface area of 401 m^2g^{-1}. The combination of such porosity along with the highly conjugated heteroatom-rich framework enabled the polymer to exhibit exceptional iodine vapor uptake of up to 314 wt % and reversible iodine adsorption in solution. Because of the inclusion of the anthracene moieties, the TALPOP exhibited excellent detection sensitivity towards iodine via florescence quenching with K_{sv} value of 2.9×10^3 L mol^{-1}. The cost effective TALPOP along with its high uptake and sensing of iodine, make it an ideal material for environmental remediation.

Nuclear energy is becoming one of the most feasible alternative sources to meet the ever-increasing energy demand and minimize the emission of greenhouse gases because of its high-density energy, minimal carbon footprints, and low operation cost[1–4]. Despite such advantages, the potential emissions of radioactive material (such as ^{129}I and ^{131}I, ^3H, $^{14}CO_2$, and ^{85}Kr) from nuclear energy power plants is a major drawback of this technology due to the serious environmental and health effect of these materials[4,5]. The long-lived radionuclides of iodine, ^{129}I (half-life of 1.57×10^7 years) and ^{131}I (half-life of ca. 8 days), are usually emitted in the gas form which then enters the food chain through contaminated air or by depositing into soil and water. The radioactive iodine isotopes have adverse effects on human metabolic system and health, and they were indicated as major cause of thyroid cancer[5–7]. Accordingly, there is an urgent need to develop new technology and means to effectively detect, capture, and store radioactive iodine.

In this context, several adsorbent materials have been studied and tested for effective sequestration and sensing of iodine[4,5,8–13]. It has been reported that iodine sequestration efficiency is a function of several structural properties of the adsorbent including surface area, pore size, specific high-affinity binding sites, polar groups, and conjugated units. Thus, increasing the affinity of the host to iodine, in addition to enhanced surface area, can have tremendous effect on iodine capture[4,5,14,15]. Materials like activated carbon, silica, silver-doped zeolites, chalcogenide aerogels, and microporous polymers have been reported to show good adsorption capacities for radioiodine[5,16,17]. However, most of these have several shortcomings such as limited surface area, high cost, low sensitivity to iodine, and difficulty in regeneration that make them quite unsuitable for practical usage[5,18–21]. For example, silver-doped zeolites are expensive and have been reported to have low adsorption capacities for iodine while metal organic frameworks, in general, are unstable in humid conditions[18–22].

Porous organic polymers (POPs), on the other hand, are another class of solid porous materials that have found applications in variety of areas that include gas storage and separation, catalysis, supercapacitors, light harvesting, and iodine capture[4,7,19,23–25]. POPs are getting increasing attention for iodine capture due to their high surface areas, versatility in design, tunable pore size and pore volumes, excellent thermal and chemical stability, and high physiochemical robustness. As such, the chemical structures of POPs can be tailor-made to incorporate heteroatoms with expanded conjugated systems in which the lone pairs on heteroatoms and the conjugated surfaces account for strong interactions between the polymers and iodine[12,15,26,27]. For example, Liu et al. reported the preparation of novel thiophene-based porous organic networks that can capture up to 204 wt.% of

[1]Department of Chemical Engineering, American University of Sharjah, P.O. Box 26666, Sharjah, United Arab Emirates. [2]Department of Biology, Chemistry, and Environmental Sciences, American University of Sharjah, P.O. Box 26666, Sharjah, United Arab Emirates. ✉email: oelkadri@aus.edu

iodine[28]. More recently, Pan et al. developed N- and S-rich covalent organic framework (COFs) possessing high iodine uptake of 276 wt.%[29]. Triazine-based conjugated polymers have also been reported to have respectable iodine uptake, presumably due to their nitrogen-rich nature[4,15,30–35]. The high number of basic nitrogen sites on the triazine unit enhances the uptake capacity that originates from the formation of charge-transfer complexes of nitrogen-iodine (donor–acceptor) systems formed during iodine adsorption on the polymers[7,12,15,36]. Geng et al. constructed a series of novel triazine-based conjugated microprous polymers (TCMPs) applying the Friedel–Crafts polymerization reactions[12,32,37,38]. The TCMPs showed remarkable iodine uptake and exhibited high detection sensitivity toward nitroaromatic compounds.

Nevertheless, despite the many reported adsorbent materials for iodine capture and storage, needs still exist for the development of new materials that are economically viable and can be prepared in a large scale with a minimal laborious synthetic protocols. Accordingly and building up on our recent reports on the use of aminal linked porous organic polymers (ALPOPs) in iodine capture and metal sensing[4,39], we envision to design and prepare multifunctional, low-cost, heteroatom-rich, and luminescent aminal linked porous organic polymer by combining nitrogen-rich triazene building block that compromises an anthracene moiety and a heterocyclic aldehyde linker. Herein, we report on the synthesis of a triazine-anthracene aminal linked porous organic polymer (TALPOP) by reacting 9,10-bis-(4,6-diamino-S-triazin-2-yl)anthracene (DTA), the core of the envisioned POP, and 2-furaldehyde, as the organic linker. The DTA building block not only offers the nitrogen-rich nature, but it also includes anthracene unit, which provides additional π-conjugated structures in the TALPOP polymeric framework, leading to positive impact on the iodine adsorption and provides good fluorescence and emission properties , which makes it a potential candidate for the development of aqueous fluorescent chemical sensors for iodine. The aldehyde linker (2-furaldehyde) is commercially available, inexpensive, and introduces additional heteroatom, thus making the resulting TALPOP ideally and economically feasible material for iodine capture and storage. The iodine uptake, release, regeneration, and adsorption kinetics were studied and reported in this work. The chemically and thermally stable novel polymer showed excellent iodine vapor uptake up to 314 wt.% and was able to release over 90% of the loaded iodine when immersed in ethanol. The TALPOP can be recycled over five times, at least, without significant loss of iodine uptake capacity. In addition, it exhibited remarkable detection sensitivity towards iodine through fluorescence quenching in dioxane with K_{sv} values as high as 2.9×10^3 L mol^{-1}.

## Experimental section

Materials, instrumentation, and methods.
DTA was prepared according to previously published procedure[40]. All other starting materials and solvents were purchased from Sigma-Aldrich and used directly as received without further purification. A EuroEA3000 series elemental analyzer was used to determine the percentage content of H, C, and N in the polymer. ^{1}H NMR spectrum of the synthesized starting material (DTA) was obtained using a Bruker-400 MHz NMR spectrometer. Fourier transfer infrared (FTIR) spectroscopy was performed on a Perkin-Elmer spectrometer having an attenuated total reflectance accessory. Thermogravimetric analysis (TGA) was performed using a Perkin-Elmer thermogravimetric analyzer under oxygen atmosphere with a heating rate of 5 °C min^{-1} and a temperature range of 30–800 °C. To obtain Scanning Electron Microscope (SEM) images of the polymer, samples were prepared by dispersing the polymer onto a sticky carbon tape attached to an aluminum sample holder. The SEM images were taken by TESCAN-LMU SEM. Powder X-ray diffraction (PXRD) patterns were collected in 2θ range of 5–50 at room temperature and scan speed of 5° min^{-1} using a Panalytical X'pert pro multipurpose diffractometer with a Cu Kα radiation. The textural properties were obtained by carrying out nitrogen adsorption–desorption experiments using a Quantachrome Autosorb iQ volumetric analyzer at 77 K. Samples weighing approximately 40 mg were degassed for 12 h at 120 °C and vacuum prior to the sorption measurements. The Brunauer–Emmett–Teller (BET) method and the non-local density functional theory (NLDFT) were used to calculate the surface area and pore size distribution. Shimadzu UV-1800 spectrometer was used to carry out UV–Vis measurements. Iodine loading capacity was determined by exposing a specific amount (40–50 mg) of the polymer in a glass vial to iodine vapor at 350 K and ambient pressure and measuring its weight before and after exposer. Weight percentages of iodine uptake were calculated by applying the following equation: $\frac{m_2 - m_1}{m_1} \times 100$wt.%, where m_1 and m_2 are masses of polymer powder before and after iodine loading, respectively. The adsorption kinetics of iodine on TALPOP (1 mg/mL) was studied at 25 °C by monitoring the removal of iodine from cyclohexane solutions at different concentrations (100 and 300 mg L^{-1}). On the other hand, the binding isotherms of TALPOP were generated by monitoring the amount of iodine adsorbed as the concentration of iodine in cyclohexane increased. Samples of the polymer (1 mg/mL) were soaked in iodine solutions with different concentrations (100, 200, 300, 400 and 500 ppm) for 72 h. The concentrations of iodine remaining in the solutions were then determined using UV–Vis absorption at 523 nm and based on calibration curves. Finally, the ability of polymer to release its encapsulated iodine was studied by placing a given amount (5 mg) of the iodine-loaded-polymer (I$_2$@TALPOP) in ethanol (15 mL) and the amount of the released iodine was monitored using UV–Vis spectroscopy. Fluorescence spectra were obtained using Edinburgh Instrument, FLS-900 scanning spectrofluorometer. The polymer was dispersed in dioxane (1 mg/10 mL) and the resulting suspension was sonicated for about 30 min at room temperature. Fluorescence spectra ($\lambda_{ex} = 389$ nm) were recorded after aliquots of iodine solution in dioxane (10 mM) were added to a quartz cuvette containing 2 mL of the suspension.

Synthesis of TALPOP.
To a 50-mL round bottom flask equipped with a condenser and magnetic stir bar, DTA (400 mg, 1.01 mmol), 2-furaldehyde (400 mg, 4.16 mmol), and DMSO (12 mL) were added. The mixture was degassed by bubbling argon for 15 min and then stirred for 3 days under argon gas at 180 °C. After cooling to room temperature, the dark precipitate was isolated using medium glass frit and subsequently washed with tetrahydrofuran (THF), acetone, methanol, and dichloromethane, and then dried under vacuum at 120 °C to
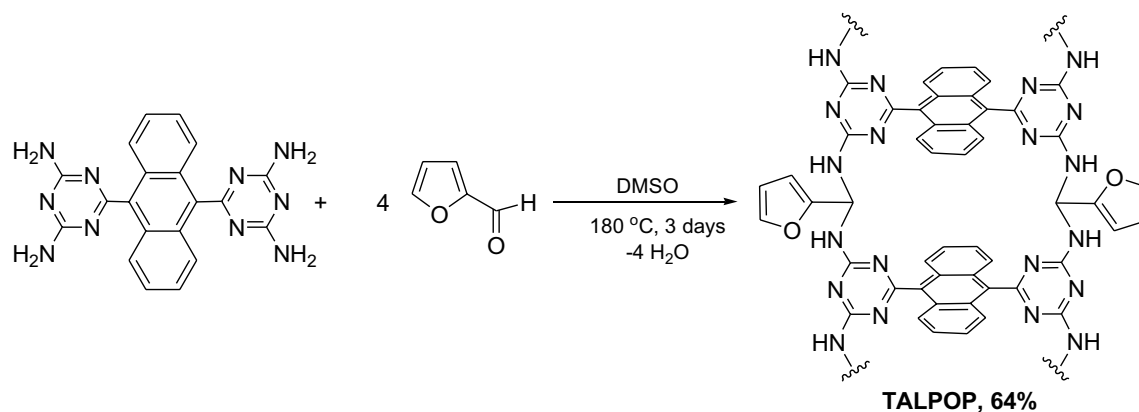
Scheme 1. Synthetic route for the preparation of the TALPOP.
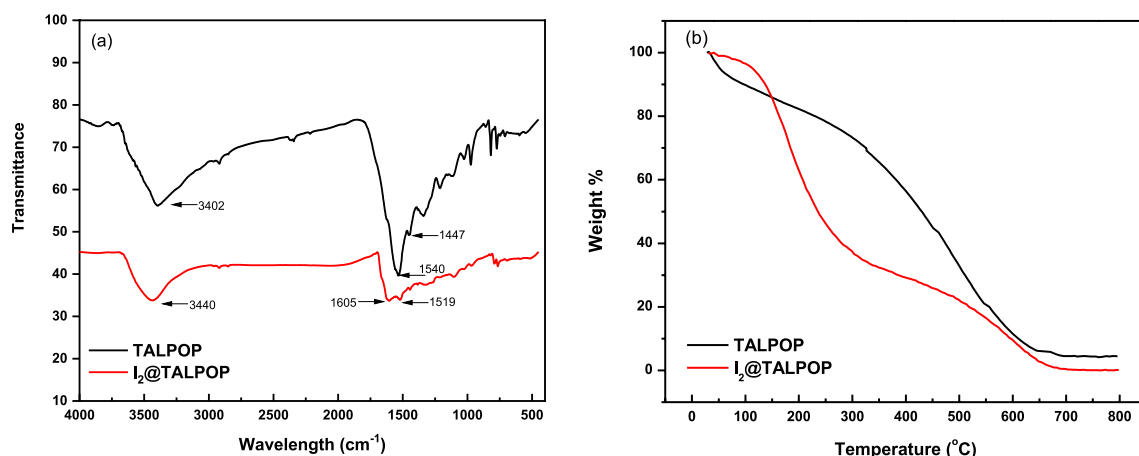
**Figure 1.** FT-IR spectrum **(a)** and TGA plots **(b)** of TALPOP and I_2@TALPOP.

afford a dark brown colored powder, TALPOP, with 64% yield. Anal. Calcd. for $C_{40}H_{32}N_{10}O_4$: C, 67.03%; H, 4.50%; N, 19.54% ; Found C, 67.41%; H, 5.60%; N, 21.00%.

Results and discussion

Synthesis and characterization. TALPOP was prepared by one-pot-Schiff base condensation reaction in high yields as dark brown powder by treating DTA with four equivalents of 2-furaldehyde in DMSO under argon atmosphere at refluxing temperature for three days (Scheme 1). The straightforward synthetic route is metal-free and does not require the addition of a catalyst. This is of significant importance not only from environmental point of view but also for economical and practical reasons. Moreover, the utilization of the commercially available, inexpensive, and biomass-based 2-furaldehyde, adds another advantage to the partially "biomass-derived" TALPOP.

The prepared TALPOP is insoluble in water, diluted acid (HCl), diluted base (NaOH), or common organic solvents such as acetone, chloroform (CHCl₃), acetonitrile, THF, dimethylformamide (DMF), 1,4-dioxane (DOX), and ethanol. Such insolubility hints to high degree of cross-linked structure and high chemical and physical stability in different environments and allows for their purification.

The structure, chemical connectivity, functional groups, crystallinity, morphology, thermal stability, and composition of TALPOP were determined using spectroscopic and analytical techniques such as FTIR, PXRD, SEM, TGA, and elemental analysis. FTIR spectra (Fig. 1a) suggests the successful formation of the TALPOP by showing a band at 3402 cm⁻¹ assigned to the stretching frequency of the secondary amine (NH) and 1540 and 1447 cm⁻¹ (quadrant and semicircle stretching) corresponding to the triazine ring. Moreover, the absence of the carbonyl groups (C=O) of the aldehydes at 1685 cm⁻¹ and primary amine (NH₂) at 3469 cm⁻¹ indicate the consumption of the functional groups (Figure S1). It is well-documented that the Schiff base reaction between amino and aldehyde functional group leads to imine (C=N) bonds. However, if the basicity of the amino groups is enhanced by electron rich substituent, for example triazene as the case in DTA, further reaction can take place between the formed imine bond and the amino groups to from stable aminal bonds (HN–CHR–NH)[7,41]. The fact that the FTIR spectra does not show peaks at around 1600 cm⁻¹ (C=N stretching vibration) and the presence of N–H stretching peak at 3402 cm⁻¹, suggests the formation of aminal linkage between the DTA and 2-furaldehyde. Such linkage formation has been confirmed for many POPs involving amino substituted triazene and aldehydes
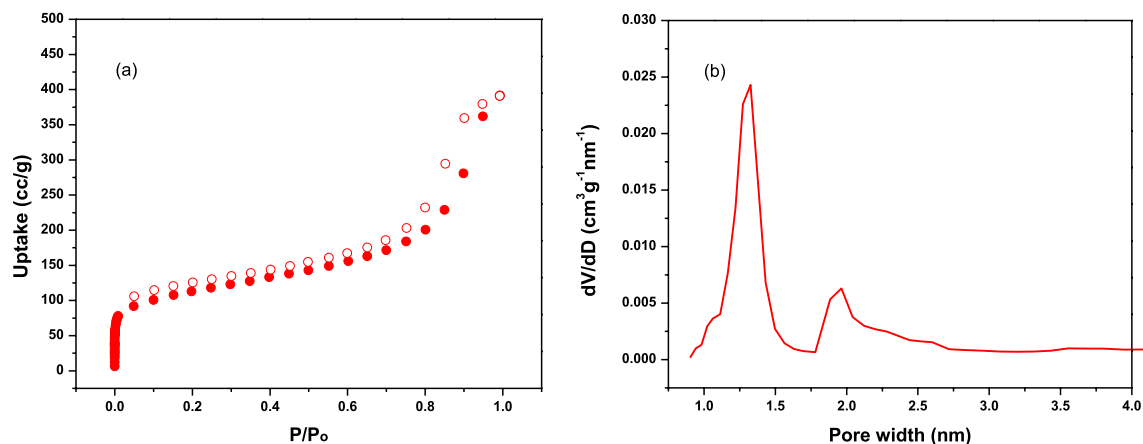
Figure 2. Nitrogen adsorption (filled spheres)-desorption (hollow spheres) isotherms **(a)** and pore size distribution **(b)** of TALPOP at 77 K.

by the use of FTIR and solid-state ^{13}C NMR techniques[7,41,42]. The synthesized TALPOP is amorphous and lack any long-range order as confirmed by PXRD (Figure S2). The amorphous nature is a well-known property for many POPs[23]. SEM images of the polymer revealed aggregates of irregular-block like structures (Figure S3 (b)). The thermal stability was assessed by TGA analysis of pristine TALPOP implying excellent thermal stability of the polymer up to ~350 °C (Fig. 1b). Initially, a weight loss of ~15% was observed at temperatures up to 100 °C attributed to the release of adsorbed water. This step was followed by a slow-rate of weight loss (~10%) up to 350 °C, attributed to the release of trapped solvent molecules in the pores of the polymer, before the onset of polymer degradation.

Porosity study. Pore characteristics and specific surface area of the TALPOP were determined through nitrogen adsorption–desorption isotherm at 77 K (Fig. 2a). The isotherm showed a steep increase in the nitrogen gas uptake at low relative pressure (P/Po < 0.01), and slower uptake at the 0.01–0.8 P/Po range, indicating the material is mostly microporous with minor mesoporous pore size distribution (PSD)[43]. The BET surface area of 401 m^{2}g^{-1} is comparable to many reported aminal linked porous organic polymers[7,33,39]. PSD (1.3 nm and 1.96 nm) and pore volume (0.871 cm^{3}g^{-1} at P/Po = 0.99) were determined using the non-local density functional theory (NLDFT) (Fig. 2b). The less than 2 nm PSD confirms the existence of a highly microporous structure.

Iodine vapor capture. In order to study the iodine capture using TALPOP, pre-weighed dried samples and excess amount of solid iodine were placed in a glass vial at 80 °C and ambient pressure in a closed system. These conditions (80 °C and ambient pressure) depict a typical nuclear fuel reprocessing unit conditions[13,37]. The amount of iodine adsorbed on the TALPOP was determined by weighing the samples at different time intervals. Figure 3 shows the iodine capture by TALPOP over a period of about three days; the results show that iodine capture was rapid in the first 8 h, after which it slowed down. There was negligible change in iodine loading weights after 24 h, suggesting saturation of the TALPOP. It is quite interesting to note that as the iodine capture by TALPOP proceeded, the color of the sample changed from brown to black (Fig. 3 inset) indicating iodine encapsulation into the polymer's framework. The equilibrium uptake of iodine by TALPOP was determined to be 3.14 g g^{-1}. The remarkable iodine uptake is among the highest value reported to date for ALPOPs[4,34,39,44]. We attribute this high uptake to the rich-heteroatom framework, large pore volume, and the large conjugated porous network represented by the anthracene moieties. To gain more insight of the interactions between the iodine molecules and the TALPOP framework, FTIR, TGA, and PXRD studies were carried out for I$_2$@TALPOP. The FTIR spectra showed that the band at 3402 cm^{-1} assigned to secondary amine (NH) shifted to 3440 cm^{-1} while the stretching frequencies of the triazine ring at 1540 and 1447 cm^{-1} changed to 1605 and 1519 cm^{-1} (Fig. 1), respectively. Such changes clearly indicate a strong interaction between the iodine molecules and TALPOP framework. Characteristic peaks of elemental iodine were not observed in the PXRD spectra (Figure S2) and thus suggesting that the iodine molecules are uniformly distributed in the framework of the TALPOP. Such uniformity was also confirmed by SEM images of the I$_2$@TALPOP (Figure S3 (b)). Moreover, no noticeable changes in the pristine TALPOP morphology after performing iodine uptake experiment suggesting that the iodine molecules are confined in the pores of the TALPOP. The TGA of I$_2$@TALPOP indicated a major weight loss between 90 and 350 °C (Fig. 1b). Since the pristine TALPOP is stable at this temperature range, it can be concluded that the weight loss is due to the release of iodine from the I$_2$@TALPOP (Fig. 1b). The 69 wt.% estimated iodine loss at 350 °C relative to the I$_2$@TALPOP is consistent with the TALPOP iodine uptake capacity where at 3.14 g g^{-1} loading capacity, 75 wt.% of I$_2$@TALPOP is iodine. It is also worth noting that the insignificant change in weight of I$_2$@TALPOP at temperatures below 100 °C (as compared to pristine TALPOP) indicates that there is insignificant amount of water adsorbed, suggesting more preference for iodine adsorption over water by the polymer.

Iodine adsorption from solution. In addition to iodine vapor capture, the TALPOP can also adsorb iodine from iodine-cyclohexane solution. Pre-weighted amounts (3 mg) of TALPOP were added to iodine solu-
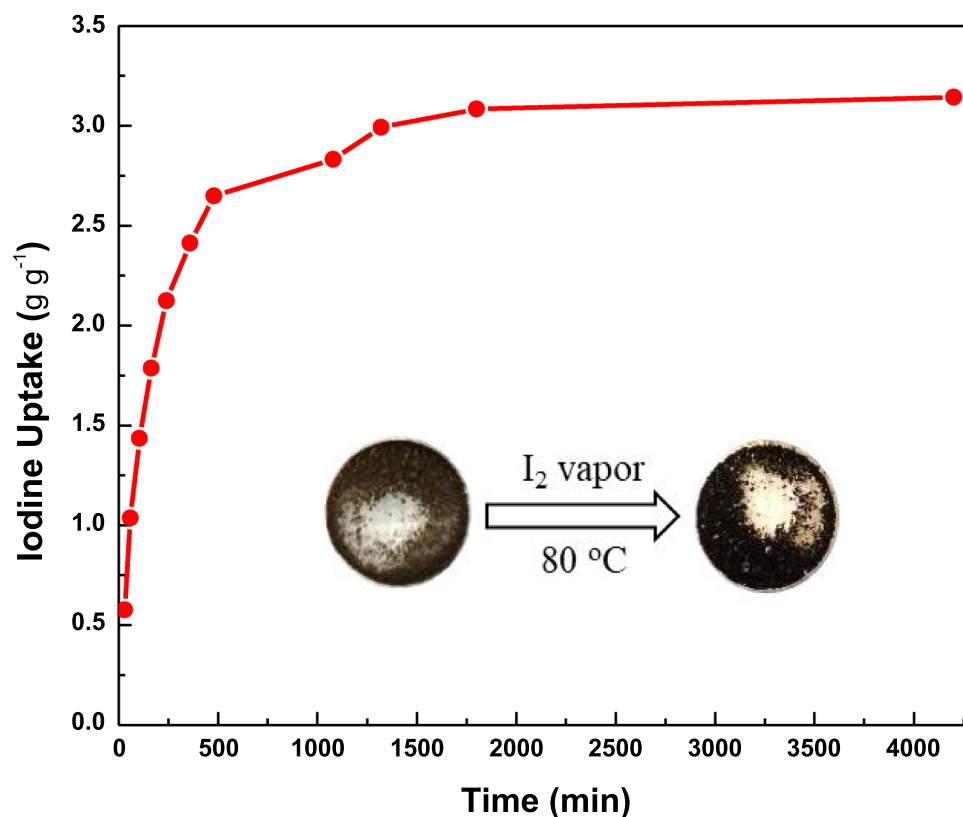
Figure 3. Gravimetric iodine uptake by TALPOP over time at 350 K and ambient pressure. Inset: photographs showing color change after the exposure TALPOP to iodine vapor.

tions (3.0 mL at 100 mg L^{-1} or 300 mg L^{-1}) in small sealed vails, and the purple colored solution faded away to very light pink over time (Fig. 4 insert) indicating the removal of iodine from the solutions. The residual amounts of iodine were monitored using UV–Vis spectroscopy. Figure 4 reveals two-stage adsorption kinetics of iodine by the TALPOP in cyclohexane solution. In stage 1, adsorption was quite rapid in the initial few hours (2–4 h) presumably due to the availability and exposure of many active sites on the polymer surface. In stage 2, there was a slow increase in the adsorption of iodine as the pores and active sites became further occupied (especially on the polymer surfaces) by iodine until equilibrium was reached. Removal efficiencies of 86% (86 mg/g uptake) and 81% (243 mg/g uptake) were recorded after 20 h for the 100 and 300 mg L^{-1} iodine-cyclohexane solutions, respectively. Such results suggest that the TALPOP is not only efficient, but also fast in removing iodine from solutions. It is obvious that the higher the initial iodine concentration, the faster the iodine uptake by the polymer, presumably due to the greater collision probability between the iodine molecules and the polymer's active sites[45]. However, the lower removal efficiency at higher initial iodine concentration is possibly due to the saturation of the pores and active sites by the large amount of iodine molecules in solution.

To further understand the kinetics of the adsorption process, the change in iodine concentration in solution over time was fitted to pseudo-first order and pseudo-second order kinetic models at 100 mg L^{-1} and 300 mg L^{-1} initial iodine concentrations (Fig. 5). The correlation coefficient R^2 values for the pseudo-first order and pseudo-second order kinetic were determined to be 0.973 and 0.999 (Table 1, S4), respectively. This suggests that the adsorption kinetics of TALPOP follows the pseudo-second order kinetic model, which indicates a chemisorption-type process[39]. Such conclusion is consistent with the presence of high interaction between the polymer surface and the iodine molecules. The existence of electron-rich heteroatoms (N, O) and aromatic rings in the polymer skeleton provide electron-donating moieties that are capable of donating electrons to the electron accepting iodine, leading to charge-transfer (CT) interaction and enhancement in iodine enrichment[46].

Adsorption isotherm for the removal of iodine by TALPOP was also constructed over an iodine initial concentration of 100–500 mg L^{-1} and at a temperature of 25 °C (Fig. 6). After soaking for 72 h with TALPOP (1 mg/mL), the residual iodine concentrations in the solutions was measured using UV–Vis spectroscopy. The obtained isotherm data (Fig. 7) was fitted to both Langmuir and Freundlich models; the former is used to model adsorption through homogenous monolayer process, while the latter is used to examine the heterogenous multilayer adsorption (S 4)[47,48]. The Langmuir isotherm (Fig. 7a) was obtained for the polymer by plotting Ce/Qe vs Ce, where Ce is the equilibrium concentration of iodine (mg/L) and Qe is the amount of iodine adsorbed per gram of TALPOP at equilibrium (mg/g). On the other hand, the Freundlich model (Fig. 7b) was applied by plotting ln(Qe) vs ln(Ce) to explore the possibility for multilayer adsorption process with reversibility.
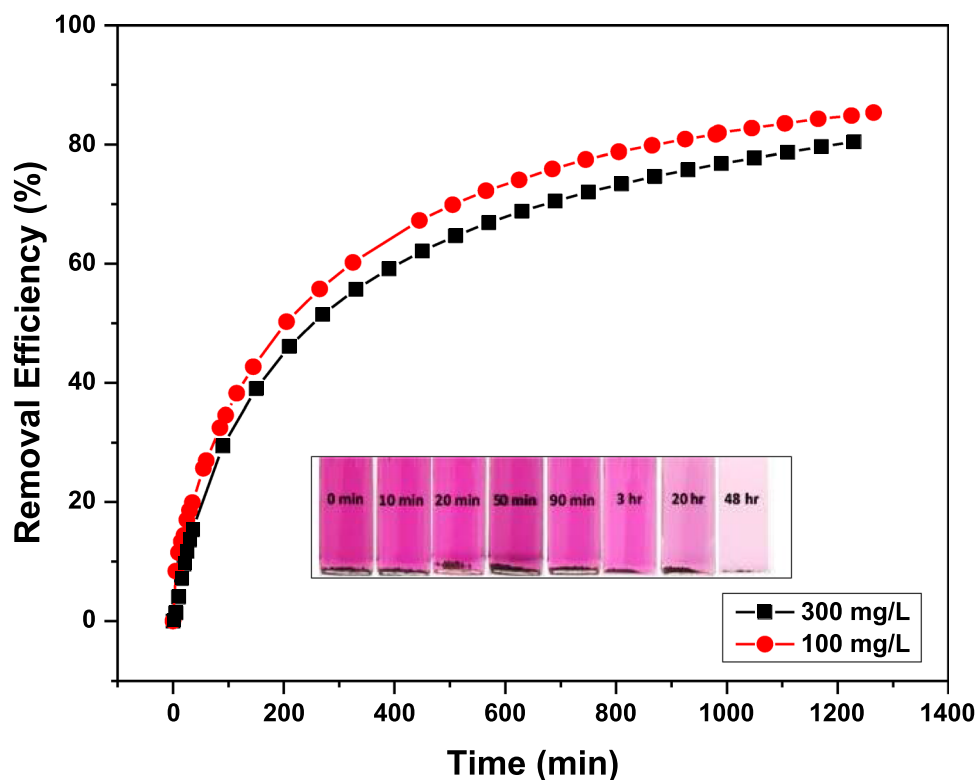
Figure 4. Kinetic studies of iodine adsorption by TALPOP in cyclohexane solution. Insert: photograph showing the change in color at different time intervals.
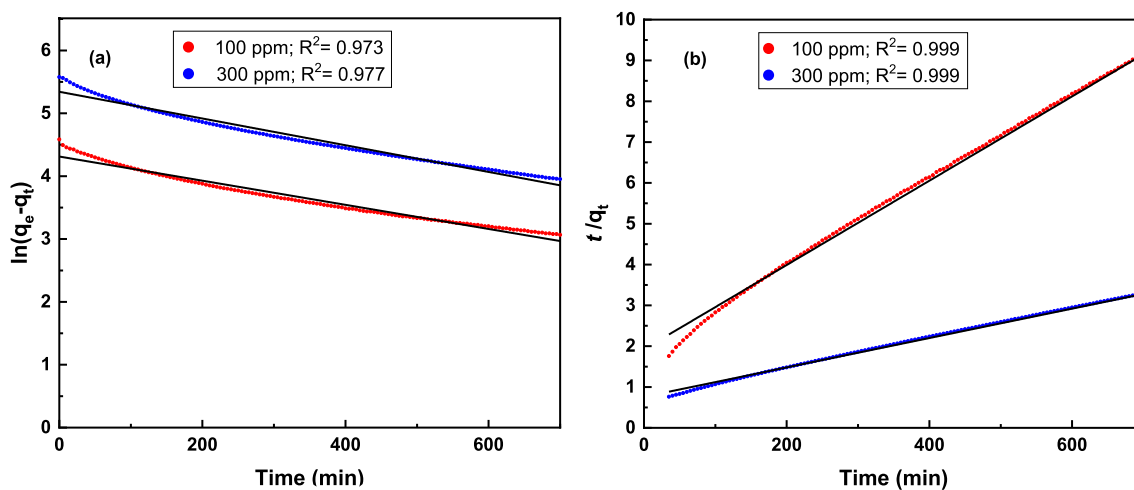

Figure 5. Pseudo First order kinetics **(a)** and pseudo second order kinetics, **(b)** of iodine adsorption on TALPOP from iodine-cyclohexane solution. The points represent the experimental data at the corresponding concentrations (100 mg/L and 300 mg/L) and the solid lines represent the corresponding model fit (temperature: 298 K; adsorbent dosage: 1 mg/mL).

The adsorption parameters are summarized in Table 2. The linear correlation coefficient value (R^2) of the Langmuir model is higher as compared to that of Freundlich model suggesting a monolayer adsorption process, presumably due to the large aromatic π-surface area. The initial part of the isotherm in Fig. 6 increases almost vertically, indicating a strong TALPOP-iodine affinity at lower concentrations to reach a maximum adsorption capacity (Q_m) calculated to be 400 mg of iodine per gram of polymer[45].

Iodine release and TALPOP regeneration. In order to test the recyclability of TALPOP, iodine release and polymer regeneration were studied using ethanol as the organic solvent. A known quantity of I$_2$@TALPOP

		Initial concentration (mg g^{-1})	
		100	300
Kinetic model	q_e (Exp) (mg g^{-1})	97.9	264.2
Pseudo-1st order	q_e (mg g^{-1})	74.6 ± 0.8	209 ± 2
	k_1 (g mg^{-1} min^{-1})	$1.92 \times 10^{-3} \pm 2.7 \times 10^{-5}$	$2.13 \times 10^{-3} \pm 2.7 \times 10^{-5}$
	R^2	0.973	0.977
Pseudo-2nd order	q_e (mg g^{-1})	96.9 ± 0.2	277.8 ± 0.6
	k_2 (g mg^{-1} min^{-1})	$5.53 \times 10^{-5} \pm 4.6 \times 10^{-7}$	$1.70 \times 10^{-5} \pm 1.2 \times 10^{-7}$
	R^2	0.999	0.999

Table 1. Kinetic parameters of pseudo-first order and pseudo-second order kinetic models. q_e adsorbed amount at equilibrium, k_1 and k_2 are the pseudo-first-order and pseudo-second-order constants, respectively, of the adsorption process.
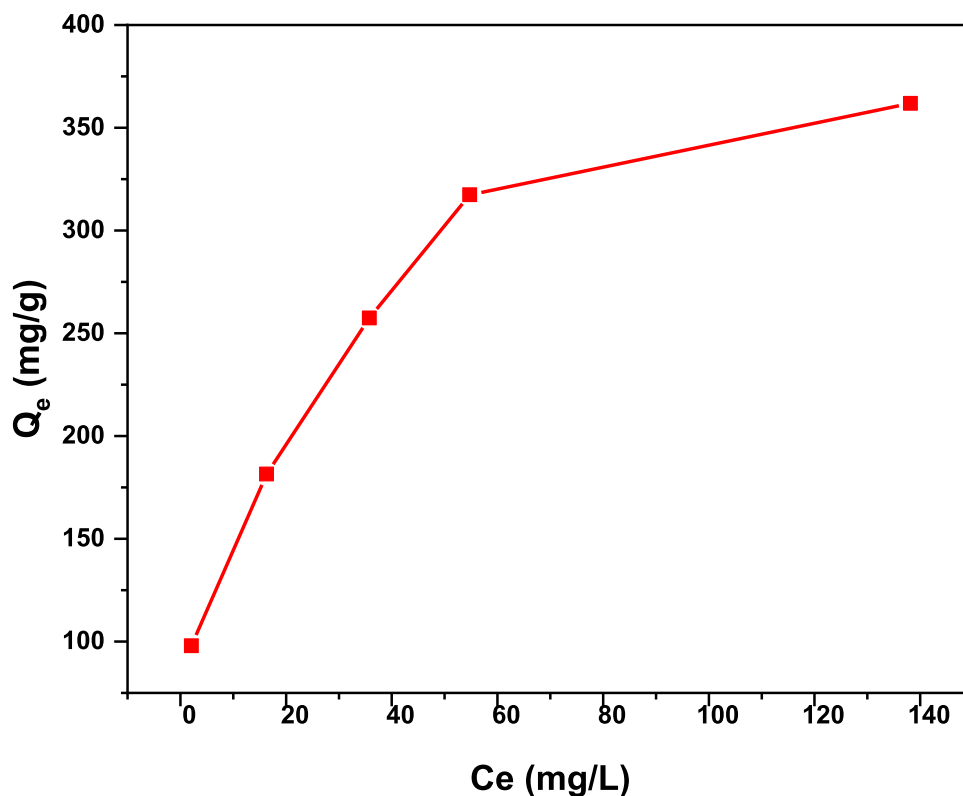
Figure 6. The adsorption isotherm of TALPOP over iodine initial concentration of 100–500 mg/L at 298 K and adsorbent dosage of 1 mg/mL.

was immersed in a known volume of ethanol for two hours at room temperature. The color of the solution changed quickly from colorless to dark brown indicating iodine transfer from the iodine encapsulated in TAL-POP to ethanol (Fig. 8a, insert). The release of iodine into ethanol was monitored using UV–Vis spectra over different time intervals. It was observed that ~ 85% of the adsorbed iodine was released within the first 20 min and almost all of the encapsulated iodine was released after two hours of incubation in ethanol (Fig. 8a). These results indicate that captured iodine can be easily removed from I$_2$@TALPOP by immersing it in ethanol and the polymer can be regenerated for another cycle of iodine adsorption. Thus, to determine the recyclability of TALPOP, a regenerated sample which, showed insignificant discoloration (Figure S4) as compared to the pristine TALPOP, was reused over five cycles for gaseous iodine uptake using similar conditions (as mentioned above). After the first cycle of adsorption-regeneration, the adsorption efficiency of the recovered TALPOP decreased by ~ 15% and only 2–3% for each of the subsequent four cycles (Fig. 8b). Thus, it can be concluded that the TALPOP can retain up to 80% of its initial iodine capture capacity after five cycles, which is comparable with many other reported POPs[26,34,39]. This also demonstrates that the TALPOP can be efficiently recycled and repeatedly utilized over many cycles without significant decline in iodine capturing capacity. Such results make TALPOP an excellent adsorbent material for practical application in the removal of radioactive iodine and provides guidelines for the design and preparation of novel POPs as adsorbents for environmental remediation.
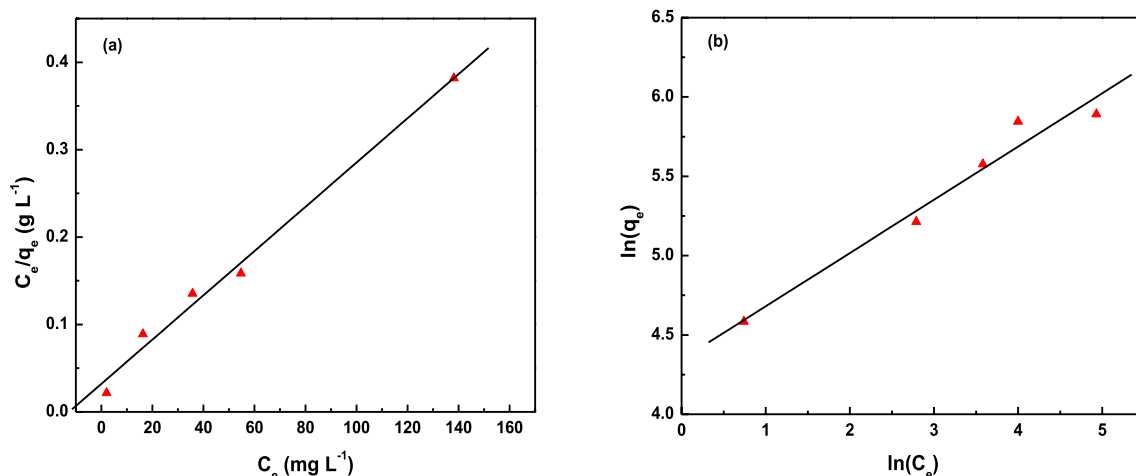
Figure 7. Fitting of adsorption isotherm data of TALPOP to Langmuir **(a)** and Freundlich **(b)** models.

| Isotherm	Parameters	
Langmuir	K_L (L/mg)	7.79×10^{-2}
	Q_m (mg/g)	400
	R^2	0.989
Freundlich	K_f (mg$^{(1-1/n)}$L$^{1/n}$/g)	76.9
	N	2.97
	R^2	0.964

Table 2. Adsorption parameters of isotherm models for iodine adsorption on TALPOP from solution. Langmiur model: Q_m = maximum monolayer coverage capacity (mg/g) K_L = Langmuir isotherm constant (L/mg) Freundlich model: K_f = Freundlich isotherm constant (mg/g).
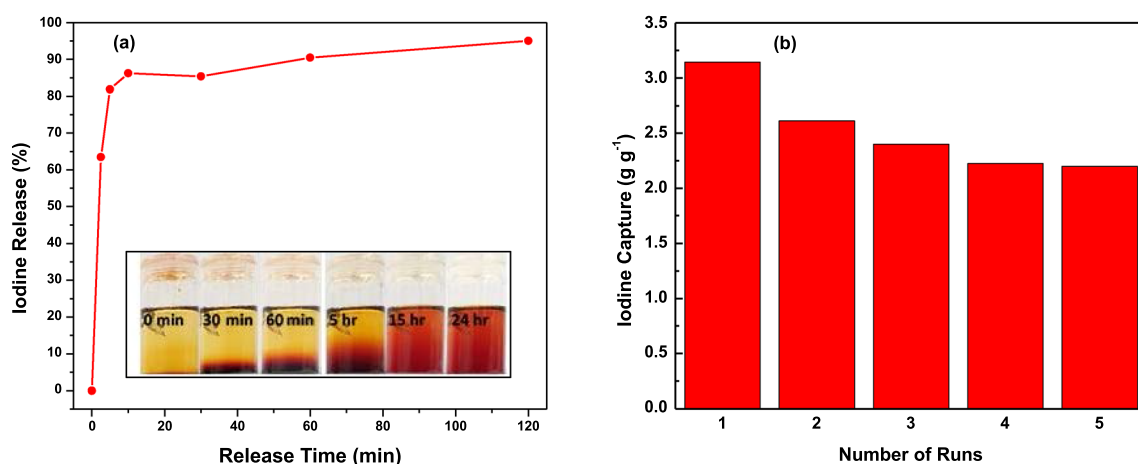
Figure 8. Release of iodine from TALPOP by immersion in ethanol **(a)** and the change in TALPOP efficiency for iodine capture by vapor sublimation upon recycling **(b)**.

Fluorescence sensing for iodine. The presence of the anthracene unit within the framework of TALPOP makes the polymer fluorescent and provides an optical probe for detecting the interaction of the guest (iodine) with the polymer. The interaction of iodine with the conjugated surface and the heteroatoms alters the electronics of the system and, hence influence the emission profile of the polymer. Thus, in order to determine the potential applications of TALPOP as fluorescent sensor for iodine in solution, samples of the polymer (0.1 mg/mL) were dispersed by sonication in some common organic solvents such as ethanol, chloroform, THF, acetone, acetonitrile, DMF, and DOX[37,38,49]. The fluorescence spectra (Figure S5) of the TALPOP is highly dependent on the solvent molecules, presumably due to the interaction of the solvent molecules with the π-conjugation structure of the TALPOP, leading to a reduced aggregation[38,50]. Among these solvents, TALPOP showed the greatest fluorescent intensity when it was dispersed in DOX (Figure S5)[37,38] and accordingly it was used as the
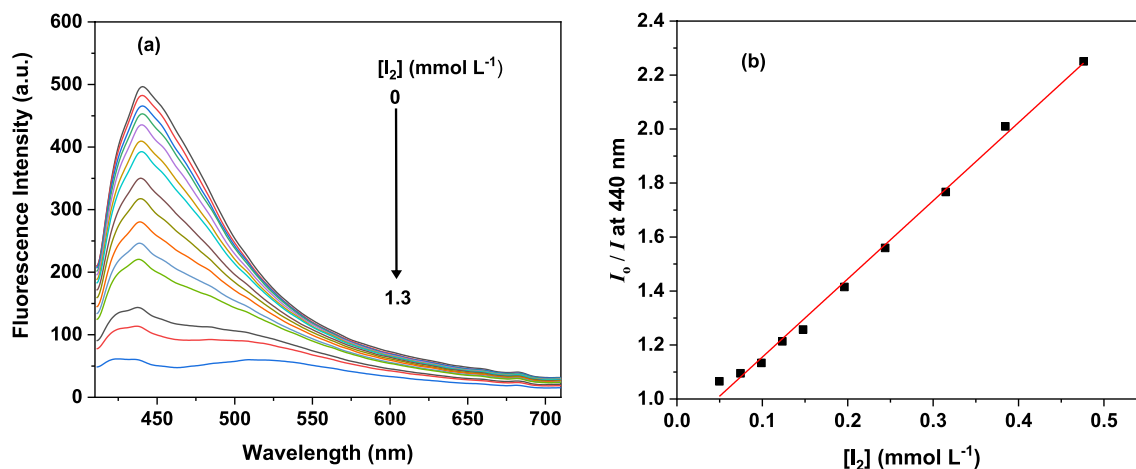
Figure 9. Fluorescent spectra (λex = 389 nm) of TALPOP upon titrating with iodine solution (0.01 mol L^{-1}) **(a)** and Stern–Volmer model fit of the relative change of fluorescent at 440 nm as iodine concentration increases **(b)**.

medium for the polymer fluorescence studies. We monitored the effect of iodine concentration in DOX on the emission of the polymer. Millimolar concentrations of iodine solutions were titrated into a uniform suspension of TALPOP in DOX (0.1 mg/mL) and the fluorescence spectra of the polymers were scanned after each addition. A systematic instantaneous decrease in the emission of TALPOP (Fig. 9a) was observed upon increase in iodine concentration. The fluorescence spectra showed a significant decrease (> 90%) in the emission as the concentration of iodine in solution increased to above 0.01 M (Fig. 9a). Thus, in order to quantify the quenching effect of iodine on the emission of the polymer, we applied the Stern–Volmer equation to determine the quenching coefficient. The Stern–Volmer plot show a good correlation between the concentration of iodine (the quencher) and the relative change in fluorescence intensity (at 440 nm) of TALPOP (Fig. 9b). The quenching coefficient (K_{sv}) for iodine was estimated to be 2.9×10^3 L mol^{-1} (S5), which is comparable with those reported for many POPs for fluorescence sensing of iodine[12,32,38]. An electron-transfer mechanism could explain the fluorescence quenching of the TALPOP. The electron-rich building block of the polymer (electron donor) and the low-lying-LUMOs of iodine (− 4.99 eV, electron acceptor), provide a driving force for electron transfer and hence quench the fluorescence[51].

Conclusions

A novel fluorescent aminal linked porous polymer was prepared via Schiff-base condensation reaction. The resulting polymer exhibits remarkable thermal and physiochemical stability presumably due to the rich π-conjugated structure. Because of such properties along with the large surface area and electron-rich nature, the polymer can capture a significant amount of iodine (3.14 g g^{-1}). The encapsulated iodine molecules can be easily released once the loaded polymer is immersed in polar solvent. The desorbed polymer showed excellent reloading capacity over 5 cycles. The aminal linked polymer also capable of removing over 85% of iodine from cyclohexane solution. In addition, it possesses excellent sensing sensitivity toward iodine with K_{sv} value of 2.9×10^3 L mol^{-1}. Results from this work suggest that aminal linked polymers are promising materials for multi-environmental applications.

References

1. Kintisch, E. Nuclear power: Congress tells DOE to take fresh look at recycling spent reactor fuel. *Science* (*80*). **310**, 1406–1406 (2005).
2. Cicia, G., Cembalo, L., Del Giudice, T. & Palladino, A. Fossil energy versus nuclear, wind, solar and agricultural biomass: Insights from an Italian national survey. *Energy Policy* **42**, 59–66 (2012).
3. Kharecha, P. A. & Hansen, J. E. Prevented mortality and greenhouse gas emissions from historical and projected nuclear power. *Environ. Sci. Technol.* **47**, 4889–4895 (2013).
4. Abdelmoaty, Y. H., Tessema, T.-D., Choudhury, F. A., El-Kadri, O. M. & El-Kaderi, H. M. Nitrogen-rich porous polymers for carbon dioxide and iodine sequestration for environmental remediation. *ACS Appl. Mater. Interfaces* **10**, 16049–16058 (2018).
5. Xie, W., Cui, D., Zhang, S.-R., Xu, Y.-H. & Jiang, D.-L. Iodine capture in porous organic polymers and metal–organic frameworks materials. *Mater. Horizons* **6**, 1571–1595 (2019).
6. Ten Hoeve, J. E. & Jacobson, M. Z. Worldwide health effects of the Fukushima Daiichi nuclear accident. *Energy Environ. Sci.* **5**, 8743–8757 (2012).
7. Song, W. C., Xu, X. K., Chen, Q., Zhuang, Z. Z. & Bu, X. H. Nitrogen-rich diaminotriazine-based porous organic polymers for small gas storage and selective uptake. *Polym. Chem.* **4**, 4690–4696 (2013).
8. Liu, S. *et al.* Efficient removal of radioactive iodide ions from water by three-dimensional Ag$_2$O-Ag/TiO$_2$ composites under visible light irradiation. *J. Hazard. Mater.* **284**, 171–181 (2014).
9. Subrahmanyam, K. S. *et al.* Ion-exchangeable molybdenum sulfide porous chalcogel: Gas adsorption and capture of iodine and mercury. *J. Am. Chem. Soc.* **137**, 13943–13948 (2015).

10. Pham, T. C. T. *et al.* Capture of iodine and organic iodides using silica zeolites and the semiconductor behaviour of iodine in a silica zeolite. *Energy Environ. Sci.* **9**, 1050–1062 (2016).

11. Chapman, K. W., Chupas, P. J. & Nenoff, T. M. Radioactive iodine capture in silver-containing mordenites through nanoscale silver iodide formation. *J. Am. Chem. Soc.* **132**, 8897–8899 (2010).

12. Geng, T., Zhu, Z., Zhang, W. & Wang, Y. A nitrogen-rich fluorescent conjugated microporous polymer with triazine and triphenylamine units for high iodine capture and nitro aromatic compound detection. *J. Mater. Chem. A* **5**, 7612–7617 (2017).

13. Qian, X. *et al.* Capture and reversible storage of volatile iodine by novel conjugated microporous polymers containing thiophene units. *ACS Appl. Mater. Interfaces* **8**, 21063–21069 (2016).

14. Sun, Q., Aguila, B. & Ma, S. Opportunities of porous organic polymers for radionuclide sequestration. *Trends Chem.* **1**, 292–303 (2019).

15. Ren, Y. Y. *et al.* Nitrogen-rich porous polyaminal network as a platform for iodine adsorption through physical and chemical interaction. *J. Appl. Polym. Sci.* **135**, 6–11 (2018).

16. Subrahmanyam, K. S. *et al.* Chalcogenide aerogels as sorbents for radioactive iodine. *Chem. Mater.* **27**, 2619–2626 (2015).

17. Zeng, M. H. *et al.* Rigid pillars and double walls in a porous metal-organic framework: Single-crystal to single-crystal, controlled uptake and release of iodine and electrical conductivity. *J. Am. Chem. Soc.* **132**, 2561–2563 (2010).

18. Mallick, A. *et al.* Fine-tuning the balance between crystallization and gelation and enhancement of CO2 uptake on functionalized calcium based MOFs and metallogels. *J. Mater. Chem.* **22**, 14951–14963 (2012).

19. Zhang, X. *et al.* Confinement of iodine molecules into triple-helical chains within robust metal-organic frameworks. *J. Am. Chem. Soc.* **139**, 16289–16296 (2017).

20. Sumida, K. *et al.* Carbon dioxide capture in metal-organic frameworks. *Chem. Rev.* **112**, 724–781 (2012).

21. Sava, D. F. *et al.* Capture of volatile iodine, a gaseous fission product, by zeolitic imidazolate framework-8. *J. Am. Chem. Soc.* **133**, 12398–12401 (2011).

22. Zhang, Z.-J. *et al.* A new type of polyhedron-based metal–organic frameworks with interpenetrating cationic and anionic nets demonstrating ion exchange, adsorption and luminescent properties. *Chem. Commun.* **47**, 6425–6427 (2011).

23. Das, S., Heasman, P., Ben, T. & Qiu, S. Porous organic materials: Strategic design and structure-function correlation. *Chem. Rev.* **117**, 1515–1563 (2017).

24. Rabbani, M. G., Sekizkardes, A. K., El-Kadri, O. M., Kaafarani, B. R. & El-Kaderi, H. M. Pyrene-directed growth of nanoporous benzimidazole-linked nanofibers and their application to selective CO2 capture and separation. *J. Mater. Chem.* **22**, 25409–25417 (2012).

25. Kassab, R. M., Jackson, K. T., El-Kadri, O. M. & El-Kaderi, H. M. Nickel-catalyzed synthesis of nanoporous organic frameworks and their potential use in gas storage applications. *Res. Chem. Intermed.* **37**, 747–757 (2011).

26. Qian, X. *et al.* Novel N-rich porous organic polymers with extremely high uptake for capture and reversible storage of volatile iodine. *J. Hazard. Mater.* **338**, 224–232 (2017).

27. Yin, Z. J. *et al.* Ultrahigh volatile iodine uptake by hollow microspheres formed from a heteropore covalent organic framework. *Chem. Commun.* **53**, 7266–7269 (2017).

28. Liu, M., Yao, C., Liu, C. & Xu, Y. Thiophene-based porous organic networks for volatile iodine capture and effectively detection of mercury ion. *Sci. Rep.* **8** (2018).

29. Pan, X. *et al.* N- and S-rich covalent organic framework for highly efficient removal of indigo carmine and reversible iodine capture. *Microporous Mesoporous Mater.* **296**, 109990 (2020).

30. Cooper, A. I. Conjugated microporous polymers. *Adv. Mater.* **21**, 1291–1295 (2009).

31. Feng, C. *et al.* Polytriazine porous networks for effective iodine capture. *Polym. Chem.* **11**, 2786–2790 (2020).

32. Geng, T., Zhang, W., Zhu, Z. & Kai, X. Triazine-based conjugated microporous polymers constructing triphenylamine and its derivatives with nitrogen as core for iodine adsorption and fluorescence sensing I2. *Microporous Mesoporous Mater.* **273**, 163–170 (2019).

33. Weng, J. Y., Xu, Y. L., Song, W. C. & Zhang, Y. H. Tuning the adsorption and fluorescence properties of aminal-linked porous organic polymers through N-heterocyclic group decoration. *J. Polym. Sci. Part A Polym. Chem.* **54**, 1724–1730 (2016).

34. Zhang, Z., Li, L., An, D., Li, H. & Zhang, X. Triazine-based covalent organic polycalix[4]arenes for highly efficient and reversible iodine capture in water. *J. Mater. Sci.* **55**, 1854–1864 (2020).

35. Zhang, G. Q., Ou, W. & Xu, Y. Sen. Fluorescein supramolecular nanosheets: A novel organic photocatalyst for visible-light-driven H2 evolution from water. *Sci. China Mater.* **61**, 1001–1006 (2018).

36. Jiang, Q., Huang, H., Tang, Y., Zhang, Y. & Zhong, C. Highly porous covalent triazine frameworks for reversible iodine capture and efficient removal of dye. *Ind. Eng. Chem. Res.* **57**, 15114–15121 (2018).

37. Geng, T. *et al.* Synthesis of tetraphenylethylene-based fluorescent conjugated microporous polymers for fluorescent sensing and adsorbing iodine. *Microporous Mesoporous Mater.* **284**, 468–475 (2019).

38. Geng, T. *et al.* Fluorescent conjugated microporous polymers containing pyrazine moieties for adsorbing and fluorescent sensing of iodine. *Environ. Sci. Pollut. Res.* 20235–20245, https://doi.org/10.1007/s11356-019-06534-8 (2020).

39. Sen, S., Al-Sayah, M. H., Mohammed, M. S., Abu-Abdoun, I. I. & El-Kadri, O. M. Multifunctional nitrogen-rich aminal-linked luminescent porous organic polymers for iodine enrichment and selective detection of Fe3+ ions. *J. Mater. Sci.* **55**, 10896–10909 (2020).

40. Rangnekar, D. W. & Rajadhyaksha, D. D. Synthesis of 9,10-bis-hetaryl anthracenes and their application on polyester fibres as disperse dyes. *J. Chem. Technol. Biotechnol.* **47**, 137–142 (2007).

41. Li, G., Zhang, B., Yan, J. & Wang, Z. The cost-effective synthesis of furan- and thienyl-based microporous polyaminals for adsorption of gases and organic vapors. *Chem. Commun.* **52**, 1143–1146 (2016).

42. Schwab, M. G. *et al.* Catalyst-free preparation of melamine-based microporous polymer networks through Schiff base chemistry. *J. Am. Chem. Soc.* **131**, 7216–7217 (2009).

43. Ben, T. *et al.* Gas storage in porous aromatic frameworks (PAFs). *Energy Environ. Sci.* **4**, 3991–3999 (2011).

44. Weng, J.-Y., Xu, Y.-L., Song, W.-C. & Zhang, Y.-H. Tuning the adsorption and fluorescence properties of aminal-linked porous organic polymers through N-heterocyclic group decoration. *J. Polym. Sci. Part A Polym. Chem.* **54**, 1724–1730 (2016).

45. Guan, H. *et al.* Adsorption behavior of iodine by novel covalent organic polymers constructed through heterostructural mixed linkers. *Front. Mater.* **6**, 12 (2019).

46. Yang, Y. *et al.* Insight into volatile iodine uptake properties of covalent organic frameworks with different conjugated structures. *J. Solid State Chem.* **279**, 120979 (2019).

47. Langmuir, I. The adsorption of gases on plane surfaces of glass, mica and platinum. *J. Am. Chem. Soc.* **40**, 1361–1403 (1918).

48. Freundlich, H. & Heller, W. The adsorption of cis- and trans-azobenzene. *J. Am. Chem. Soc.* **61**, 2228–2230 (1939).

49. Yuan, K. *et al.* Nanofibrous and graphene-templated conjugated microporous polymer materials for flexible chemosensors and supercapacitors. *Chem. Mater.* **27**, 7403–7411 (2015).

50. Hayashi, S. *et al.* Synthesis of π-conjugated network polymers based on fluoroarene and fluorescent units via direct arylation polycondensation and their porosity and fluorescent properties. *J. Polym. Sci. Part A Polym. Chem.* **55**, 3862–3867 (2017).

51. Geng, T. *et al.* Poly[1,3,6,8-tetra(2-thiophenyl)pyrene] and poly[1,3,6,8-tetra(3-thiophenyl)pyrene] conjugated microporous polymers for reversible adsorbing and fluorescent sensing iodine. *J. Polym. Res.* **26**, 1–10 (2019).

Author contributions

O.M.E.-K. conceived the original idea, analyzed the data, and finalized the manuscript. M.H.A. designed the methods and helped in analyzing the data and finalizing the manuscript. M.A.S. and S.S. carried out the experiments and contributed to the first draft of the manuscript. T.H.I. contributed in finalizing the manuscript.

Competing interests

The authors declare no competing interests.

Additional information

Supplementary information is available for this paper at https://doi.org/10.1038/s41598-020-72697-x.

Correspondence and requests for materials should be addressed to O.M.E.-K.

Reprints and permissions information is available at www.nature.com/reprints.

Publisher's note Springer Nature remains neutral with regard to jurisdictional claims in published maps and institutional affiliations.